Supplementary information

A Novel Bio-Electrochemical Sensor Based on 1,4-Bis (Triphenylphosphonium)Butane))$_3$[$SiW_{11}O_{39}Ni(H_2O)$]/P@ERGO Nanocomposite for the Selective Determination of L-Cysteine and L-Tryptophan

Saeide Ahmadi Direstani; Somayeh Dianat*

Department of Chemistry, Faculty of Sciences, University of Hormozgan, Bandar Abbas 79161-93145, Iran

Characterization

The micro-structural information about conjugated and carbon-carbon bonds of synthesized graphene oxide (GO) were determined by Raman spectroscopy. Figure 1S displays the Raman spectrum of GO. From spectrum it is observed that GO revealed an excitation wavelength at 495 cm^{-1} and a D band at 1389 cm^{-1} credited to the structural defect (partially disordered) of the aromatic carbon-carbon bonds, and a large G band at about 1609 cm^{-1} due to the sp^2 carbon bond stretching reveals the lattice distortions. Another peak 2D and D+G is a defect activated peaks also visible at about 2821 cm^{-1} and 2934 cm^{-1}.

The FT-IR spectra of $SiW_{11}Ni$, (BTPB)$SiW_{11}Ni$, and (BTPB)$SiW_{11}Ni$/GO (Figure 2S.) exhibit characteristic peaks of Keggin structure, corresponding to the stretching vibrations of Si-O_a, W-O_b-W, W-O_c-W, and W-O_d. The existence of these stretching vibration peaks in (BTPB)$SiW_{11}Ni$ and (BTPB)$SiW_{11}Ni$/GO verify that the parent POM in the hybrid compounds has kept its Keggin structure. Furthermore, the stretching bands about 1580, 1440, 1108, and 1112 cm^{-1} in (BTPB)$SiW_{11}Ni$/GO, which are related to the stretching vibrations of C = C aromatic, C-O, and P-C, approve the presence of BTPB and GO (compare curve e with c and d). The FT-IR data are summarized in Table 1S.

The XRD patterns of $SiW_{11}Ni$, (BTPB)$SiW_{11}Ni$, BTPB, GO, and (BTPB)$SiW_{11}Ni$/GO are shown in Figure 3S. As presented in Figure 3S-b, (BTPB)$SiW_{11}Ni$ displays a diffraction peak at 8.3° as (001) and 18.4° as (002) of the $SiW_{11}Ni$ (Figure 3S-a). Other sharp characteristic peaks at 10.2°, 22.3, 25.5, and 27.7° can be

Corresponding author:
*Tel.: +98 76 33670121, Email Address: s.dianat@hormozgan.ac.ir

indexed to the BTPB (Figure 3S-c). The XRD pattern of the GO is shown in Figure 3S-d. Two fairly broad peaks appeared at 7.6° and 25.6° that match with (001) and (002) diffraction peaks of GO and graphite in the structure of GO, respectively. The (BTPB)$SiW_{11}Ni$/GO (Figure 3S-e) shows a sharp peak at 7.1° that corresponds to the $SiW_{11}Ni$ species. This result confirms that the Keggin structure of $SiW_{11}Ni$ is preserved in the hybrid nanocompound. Moreover, the board peak of about 27.2° (002) confirmed that (BTPB)$SiW_{11}Ni$ was immobilized onto the GO surface. However, the (001) diffraction peak was not detected due to the peak overlap with the $SiW_{11}Ni$, which has a greater crystallinity.

The TEM images of the GO and (BTPB)$SiW_{11}Ni$/GO at the different magnifications are shown in Figure 4S. TEM images of (BTPB)$SiW_{11}Ni$/GO indicate a homogeneous dispersion of (BTPB)$SiW_{11}Ni$ nanospheres into the GO surface, thereby improving its electrochemical behavior.

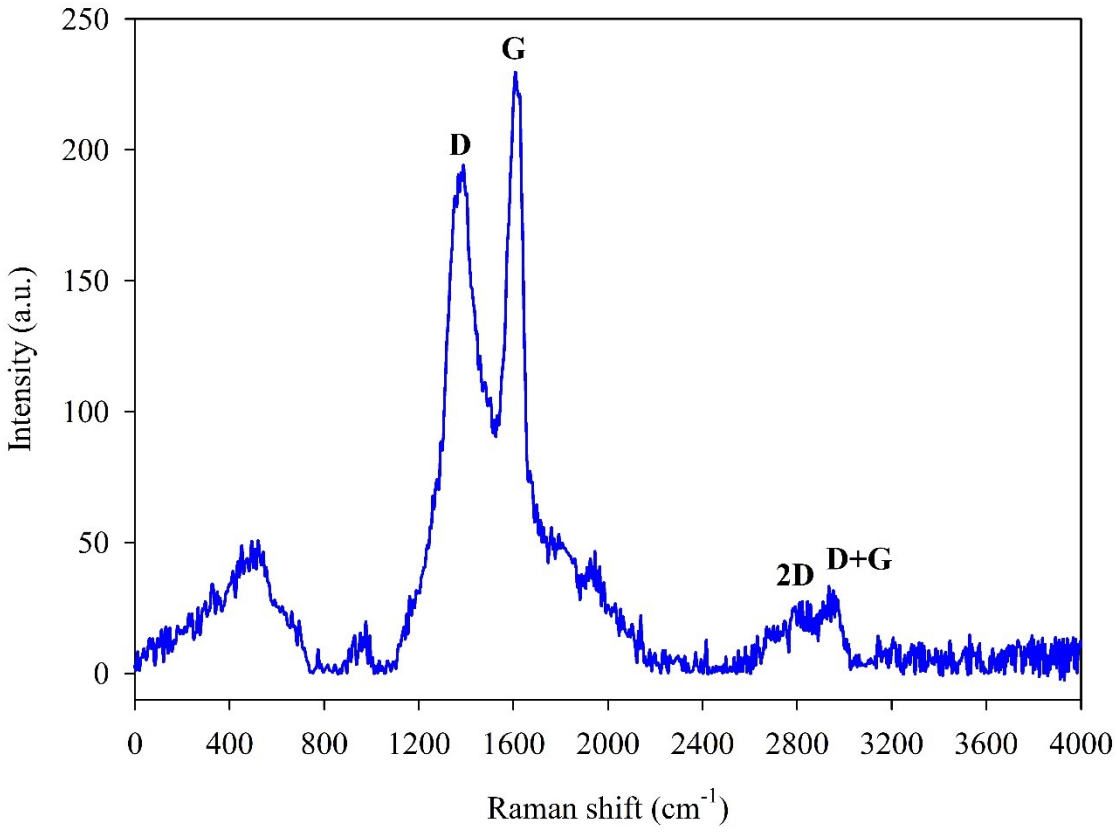

Figure 1S. Raman spectrum of synthesized graphene oxide (GO)

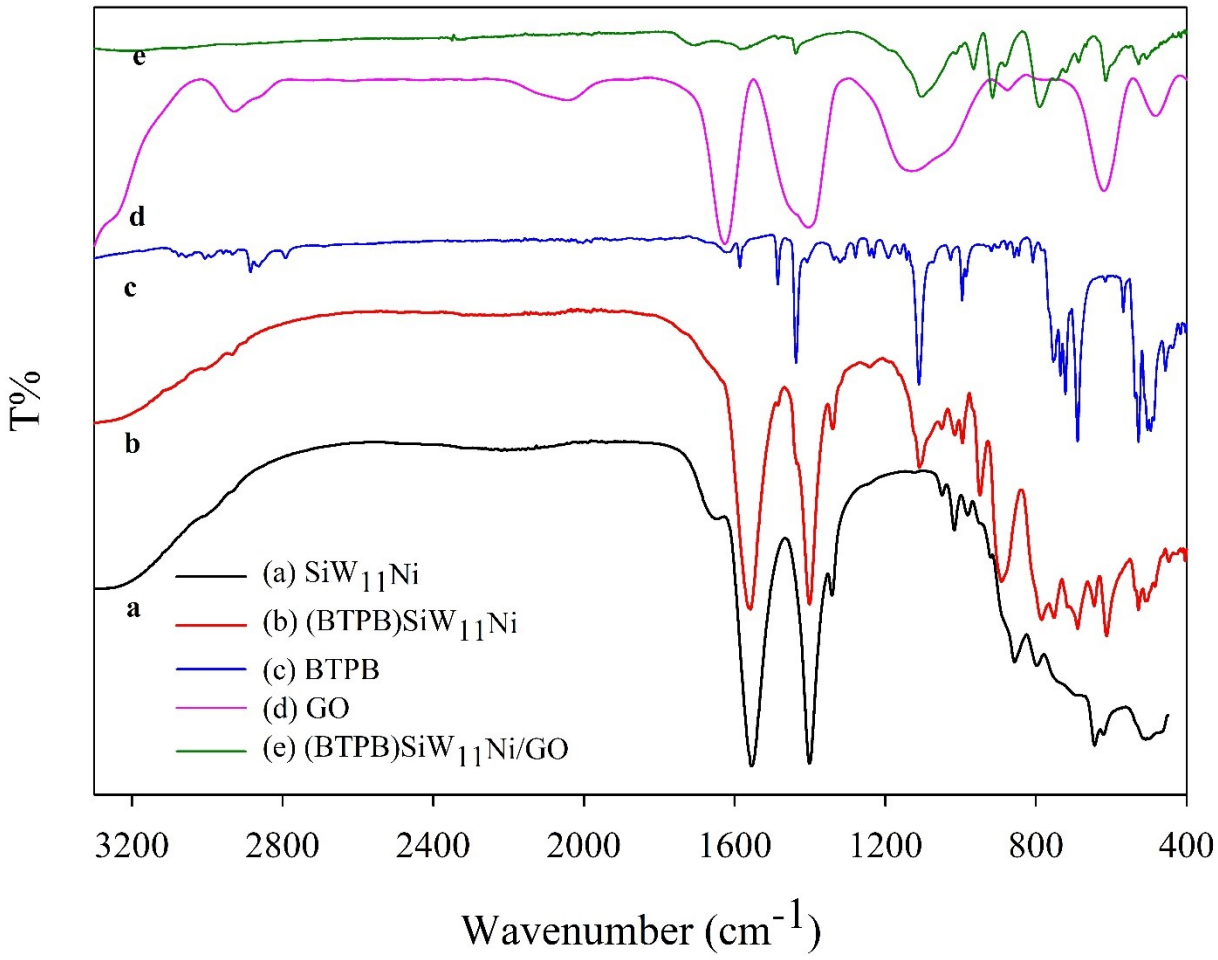

Figure 2S. FT-IR spectra of (a) $SiW_{11}Ni$, (b) $(BTPB)SiW_{11}Ni$, (c) BTPB, (d) GO, and (e) $(BTPB)SiW_{11}Ni/GO$

Table 1S. FT-IR data ($\bar{\upsilon}/cm^{-1}$) of $SiW_{11}Ni$, $(BTPB)SiW_{11}Ni$, BTPB, GO, and $(BTPB)SiW_{11}Ni/GO$

Compound	$\bar{\upsilon}$(C=C)	$\bar{\upsilon}$(C-O)	$\bar{\upsilon}$(P-C)	$\bar{\upsilon}$(Si-O_a)	$\bar{\upsilon}$(W-O_d)	$\bar{\upsilon}$(W-O_b-W)	$\bar{\upsilon}$(W-O_c-W)
$SiW_{11}Ni$	-	-	-	1018	983	857	797
BTPB	1483, 1440	-	1115, 998	-	-	-	-
$(BTPB)SiW_{11}Ni$	1486, 1440	-	1112, 995	1017	952	894	793
GO	1627, 1402	1130	-	-	-	-	-
$(BTPB)SiW_{11}Ni/GO$	1585, 1440	1108	1112	1017	968	918	796

O_a Central oxygen
O_b, O_c Bridging oxygen
O_d Terminal oxygens

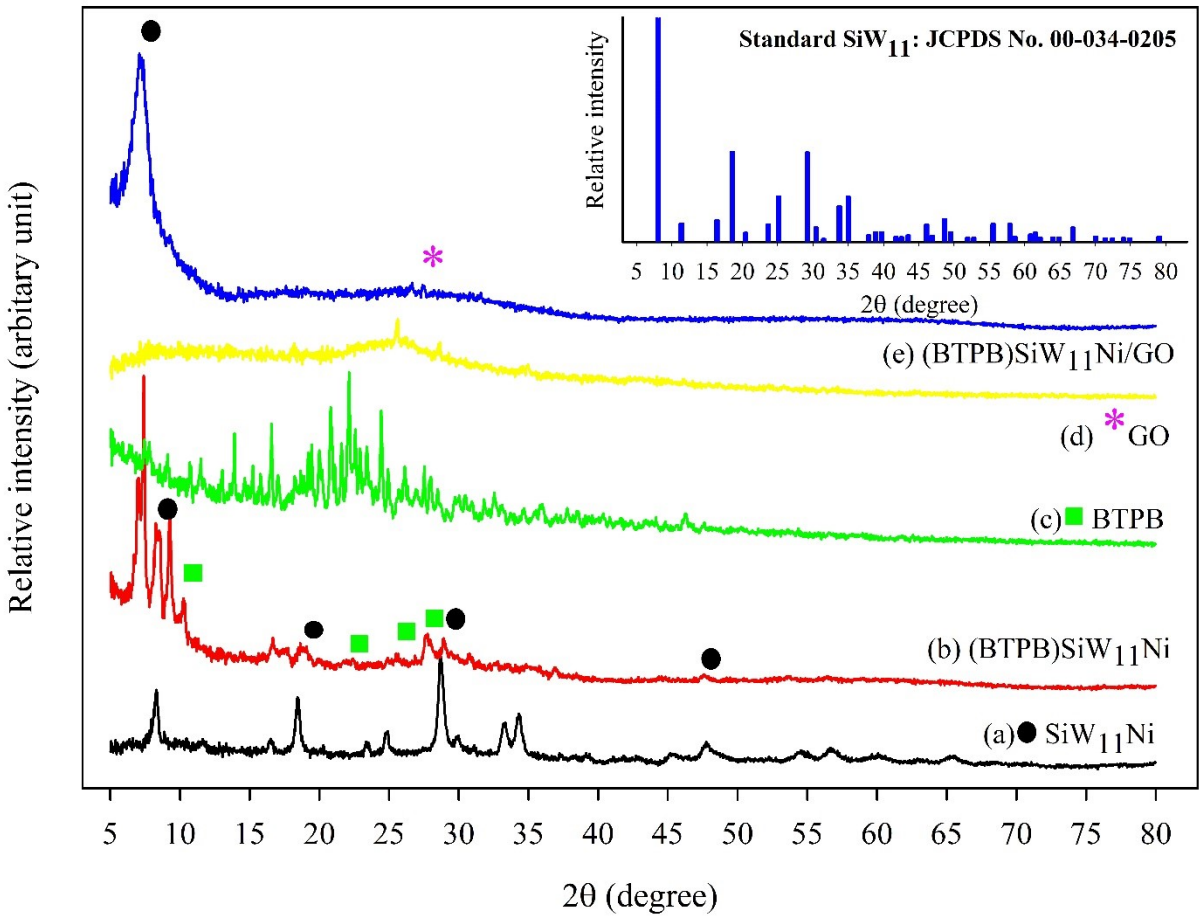

Figure 3S. XRD patterns of (a) $SiW_{11}Ni$, (b) $(BTPB)SiW_{11}Ni$, (c) BTPB, (d) GO, and (e) $(BTPB)SiW_{11}Ni/GO$. The inset shows the standard XRD pattern of $SiW_{11}O_{39}$ (SiW_{11}).

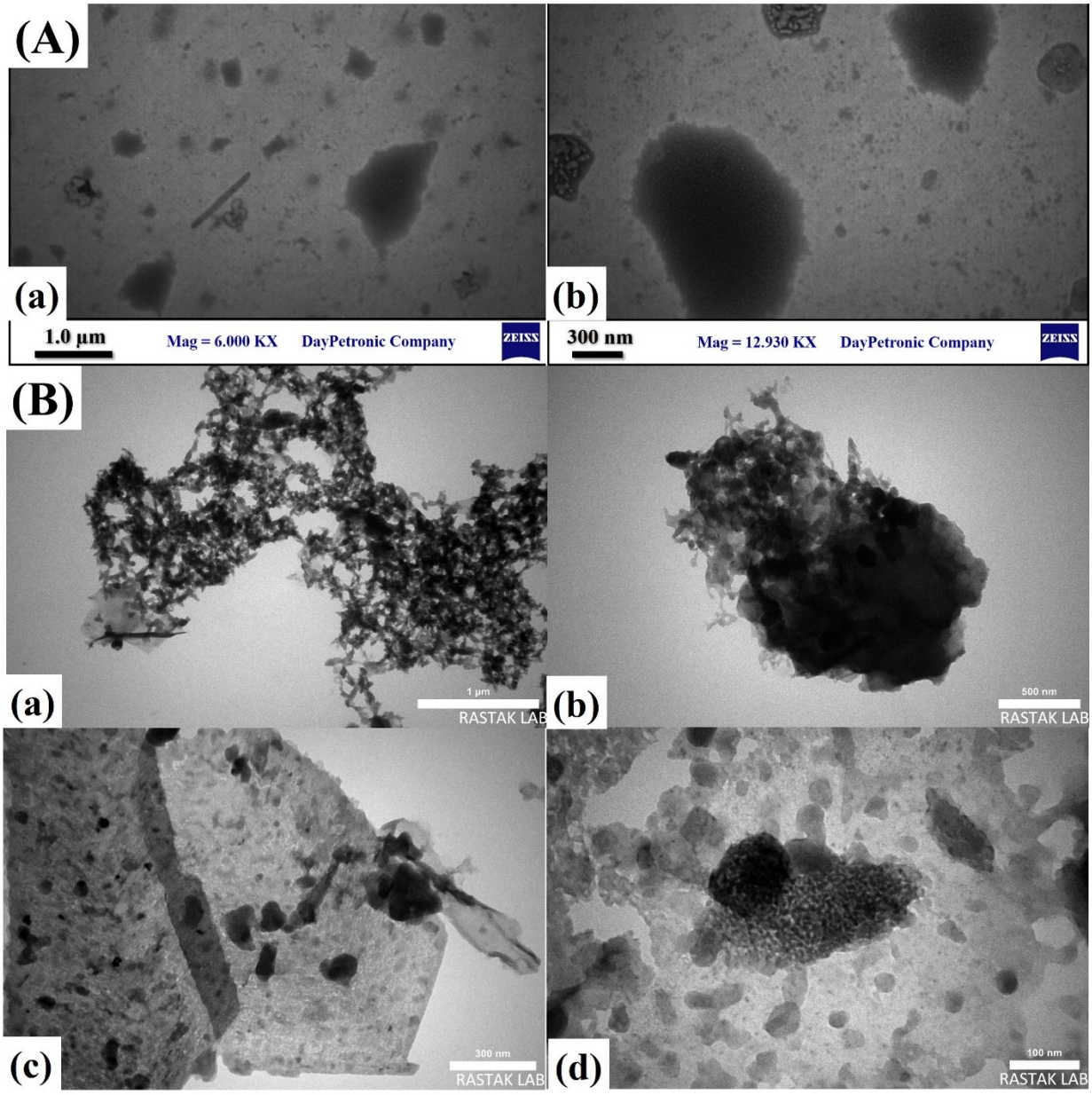

Figure 4S. TEM images of (A) GO (a, b) and (B) (BTPB)$SiW_{11}Ni$/GO (a, b, c, d) at different magnifications**.**

Parameters optimization for (BTPB)$SiW_{11}Ni$/P@ERGO/GCE coating

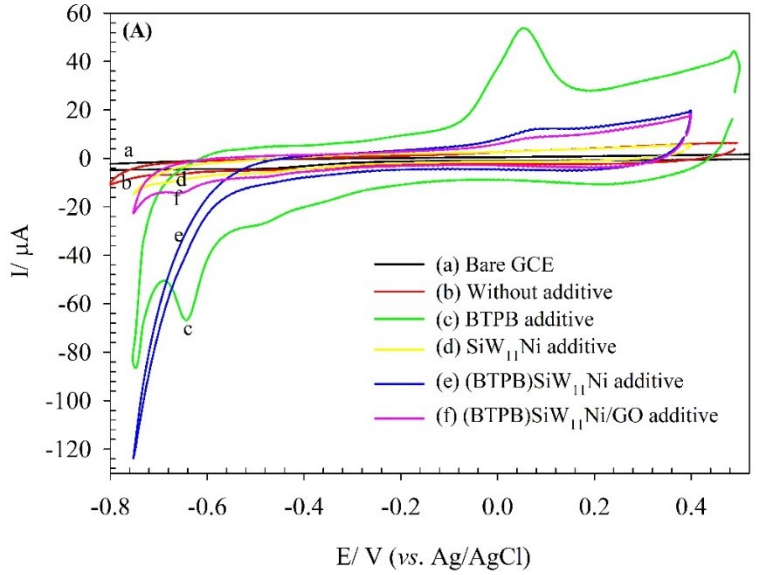

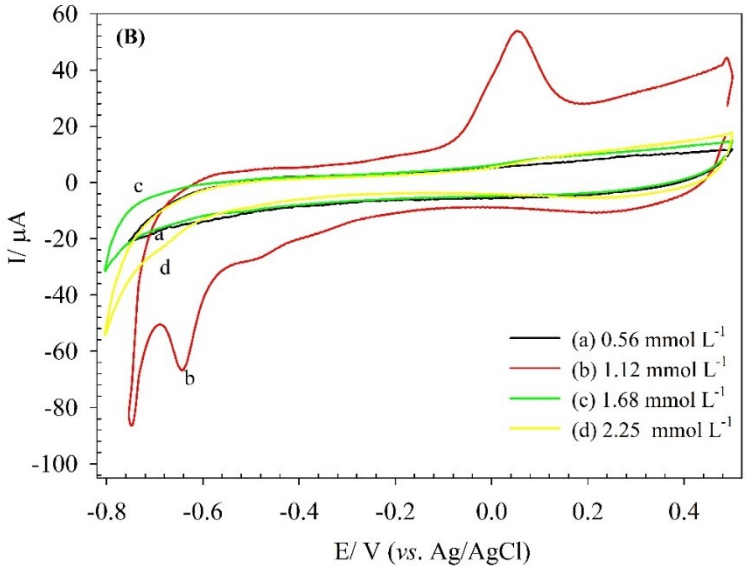

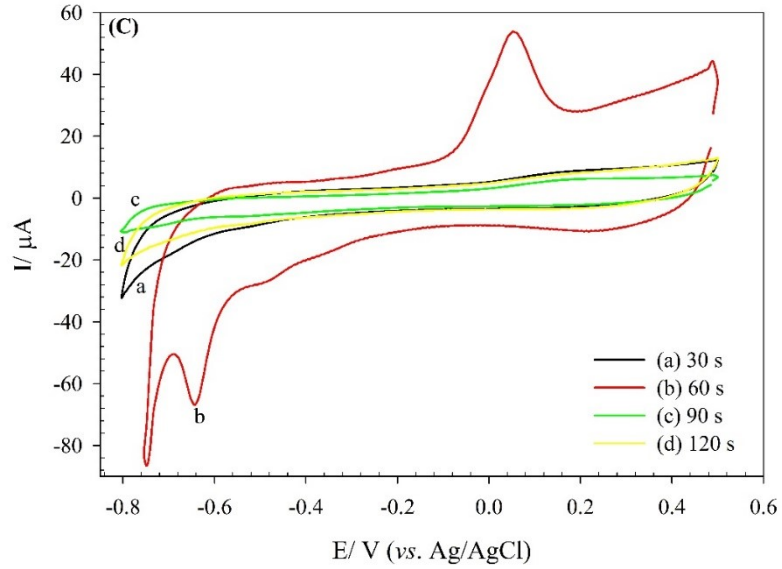

Figure 5S. Effect of (A) electrolyte additive type, (B) concentration of BTPB additive, (C) deposition time in 0.1 mol L^{-1} H_3PO_4; potential of -1.5 V; in 0.5 mol L^{-1} H_2SO_4, scan rate 100 mV s^{-1}, on the electrochemical properties of (BTPB)$SiW_{11}Ni$/P@ERGO/GCE.

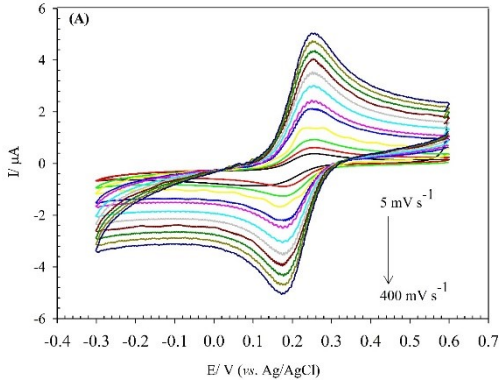
(A)
I/ µA
E/ V (vs. Ag/AgCl)
5 mV s-1
400 mV s-1

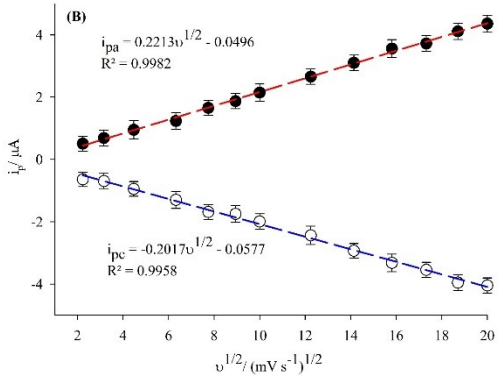
(B)
ipa = 0.2213υ1/2 - 0.0496
R² = 0.9982
ipc = -0.2017υ1/2 - 0.0577
R² = 0.9958
ip/ µA
υ1/2/ (mV s-1)1/2

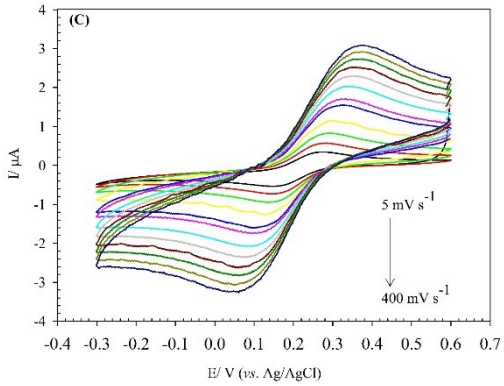
(C)
I/ µA
E/ V (vs. Ag/AgCl)
5 mV s-1
400 mV s-1

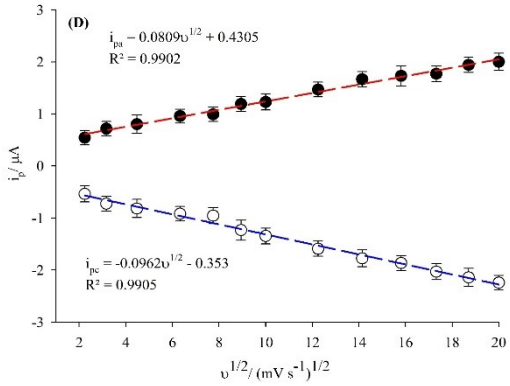
(D)
ipa = 0.0809υ1/2 + 0.4305
R² = 0.9902
ipc = -0.0962υ1/2 - 0.353
R² = 0.9905
ip/ µA
υ1/2/ (mV s-1)1/2

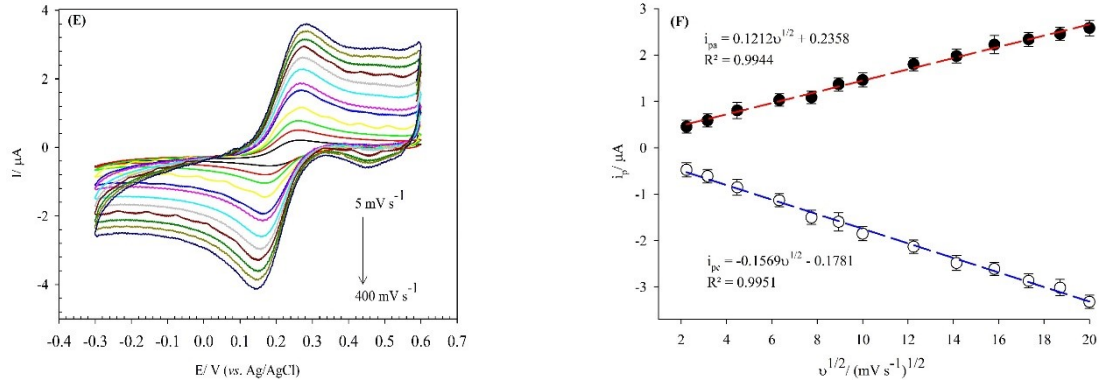

Figure 6S. CVs obtained in the presence of $[Fe(CN)_6]^{3-/4-}$ (0.5 mmol L^{-1}) redox probe On the (A) BTPB/GCE, (C) $SiW_{11}Ni$/GCE, and (E) (BTPB)$SiW_{11}Ni$ at different scan rates from 5 to 400 mV s^{-1}. Variations of the anodic, and cathodic peak currents on the (B) BTPB/GCE, (D) $SiW_{11}Ni$/GCE, and (F) (BTPB)$SiW_{11}Ni$ with square root of scan rates.

Stability, repeatability, and reproducibility of the (BTPB)SiW_{11}Ni/P@ERGO/GCE

One of the main goals of analytical electrochemistry is to achieve a sensor or bio-sensor with high stability. On the other hand, the POM-based modified electrodes ordinarily have low stability in aqueous solutions because POMs can simply permeate from the surface of modified electrode into the electrolyte. Therefore, the stability of the (BTPB)SiW_{11}Ni/P@ERGO/GCE is one crucial parameter that must be evaluated. The stability of this bio-sensor was estimated using the amperometry technique in 0.01 mol L^{-1} PBS (pH 7) The result was presented in the electronic supplementary information (Figure 7S-A). Moreover, the long-term stability of the bio-sensor was evaluated by SWV measurements under ambient air over a period of four weeks. The results were shown in the electronic supplementary information (Figure 7S-B). As shown in Figure 7S-B, the peak I' current of the bio-sensor remained at 96.03% of its initial current after one week, 91.19 % after two weeks, 88.97 % after three weeks and 87.17 % after four weeks. The high stability of the bio-sensor can be ascribed to the presence of BTPB and immobilization of the (BTPB)SiW_{11}Ni hybrid compound on the GO surface, which decreases solubility of POM in aqueous solutions.

To investigate the repeatability of the (BTPB)SiW_{11}Ni/P@ERGO/GCE, six different SWV measurements with one modified GCE were performed in 0.01 mol L^{-1} PBS (pH 7). Furthermore, six modified GCE were prepared under identical conditions to validate the reproducibility. The measurements' relative standard deviation (RSD) for the repeatability and reproducibility were 2.02% and 4.23%, respectively, demonstrating excellent precision for the fabricated bio-sensor. The obtained repeatability and reproducibility results are shown in Figures 7S-C and 7S-D, respectively.

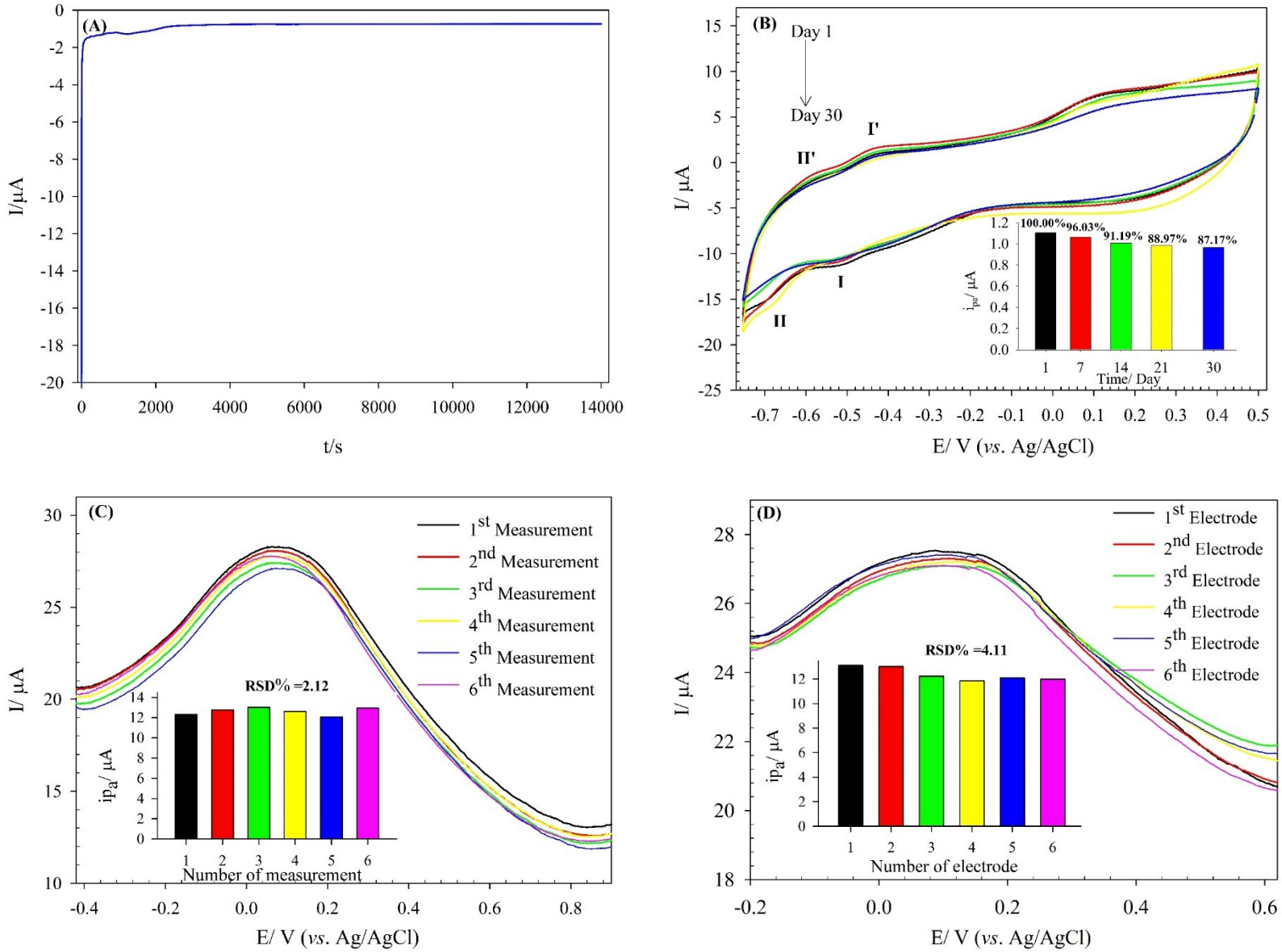

Figure 7S. (A) Stability investigation of (BTPB)$SiW_{11}Ni$/P@ERGO/GCE in PBS (0.01 mol L^{-1}, pH 7) by chronoamperometry (I-t) measurement at the fixed-potential of -0.44 V (B) Long-term stability of (BTPB)$SiW_{11}Ni$/P@ERGO/GCE in PBS (0.01 mol L^{-1}, pH 7) during a period of 30 days, (C) Repeatability test of (BTPB)$SiW_{11}Ni$/P@ERGO/GCE in PBS (0.01 mol L^{-1}, pH 7) by SWV; Step potential 2 mV, Amplitude potential 20 mV ,

inset shows histogram of the peak current of each measurment, and (D) Reproducibility test of (BTPB)$SiW_{11}Ni$/P@ERGO/GCE in PBS (0.01 mol L^{-1}, pH 7) by SWV; Step potential 2 mV, Amplitude potential 20 mV, inset shows histogram of the peak current of each modified GCE.